Instantaneous Structure of Vortex Breakdown on a Delta Wing via Particle Image Velocimetry

J. Towfighi* and D. Rockwell†
Lehigh University, Bethlehem, Pennsylvania 18015

I. Introduction

An important feature of flow past delta wings and bodies of revolution at high angle of attack is the onset of vortex breakdown within the leading-edge vortex. In recent decades, considerable attention has been focused on theoretical and experimental descriptions of various aspects of the vortex breakdown process, as reviewed by Hall,[1] Leibovich,[2,3] Escudier,[4] and Brown and Lopez.[5] From an experimental standpoint, the characterization of breakdown using qualitative flow visualization or time-averaged pointwise measurements has provided valuable insight. Certain issues, however, are difficult to resolve with qualitative flow visualization. Examples include the direction of swirl of the instability arising at the onset of breakdown and the mode (bubble vs spiral) of breakdown. An in-depth understanding of the onset and development of breakdown requires, therefore, quantitative experimental characterization of the instantaneous structure of the region of vortex breakdown. Such an experimental approach could provide interpretations analogous to those attainable with direct numerical simulation (Visbal[6]). Moreover, regions of breakdown exhibit phenomena that are typically modulated by low-frequency undulations; such low-frequency events can be characterized effectively using a whole field, experimental approach that selectively samples over longer time intervals. Particularly important is the determination of the instantaneous vorticity, which is invariant with reference frame and provides an unambiguous representation of the flow structure. Consideration of the vorticity field is further motivated by the recent theoretical model of Brown and Lopez.[5] In contrast to previous criteria for vortex breakdown, which are based on the ratio of the axial to azimuthal velocity components, Brown and Lopez[5] emphasize the crucial role of both the velocity and vorticity helix angles. According to their model, the onset of negative azimuthal vorticity is a necessary condition for the onset of vortex breakdown.

The overall objective of this investigation is to characterize the instantaneous structure of vortex breakdown over an entire plane of the flow by means of high density particle image velocimetry (PIV), using an approach described by Rockwell et al.,[7] in which some preliminary features of the instantaneous structure of vortex breakdown were reported. This investigation focuses on determination of the instantaneous contours of azimuthal vorticity and sectional streamline patterns over a plane passing through the centerline of the leading-edge vortex on a delta wing. The flow structure is characterized as a function of time after the wing is abruptly brought to a stationary position following a transient pitching motion.

II. Experimental System and Approach

Experiments were performed in a large-scale water channel, having cross-sectional dimensions 915 mm wide by 560 mm deep. The freestream velocity was 50.8 mm/s. The delta wing employed in the experiment had a sweep angle of 75 deg and a chord of 246 mm, giving a value of Reynolds number based on a chord of 1.13×10^4. It was driven by a computer-controlled motor in a pitching motion about its midchord from an initial angle of attack of $\alpha = 15$ deg to a final value of 40 deg at a dimensionless pitching rate $\dot{\alpha}C/2U = 0.15$. Of primary interest in this investigation is the development of the flow following cessation of the wing motion at $\alpha = 40$ deg. During this time, the location of vortex breakdown moves upstream toward the apex of the wing. The camera was triggered every second to provide the time history of the vortex response.

The instantaneous velocity field over an entire plane of the flow, which permitted calculation of the instantaneous contours of azimuthal vorticity and the corresponding sectional streamline patterns, was obtained using a laser-scanning version of high-image-density particle image velocimetry, as described by Rockwell et al.[8] The laser sheet, which was oriented such that it cut through the centerline of the leading-edge vortex at $\alpha = 40$ deg, was generated by a system involving a 2-W argon-ion laser and a multi-(72) faceted mirror that provided an effective pulsing of the laser sheet by rapidly scanning it across the plane of interest. The 35-mm negatives of the multiple particle images were interrogated using a fringe analysis system, whereby the first Fourier transform is performed optically and the second one digitally. The diameter d_I of the laser interrogation beam was 1.0 mm and the magnification M was 0.152, giving $d_I/M = 6.57$ mm in the plane of the laser sheet. To satisfy the Nyquist criterion, the step size Δl of the interrogation process was 0.5 mm, i.e., $\Delta l = 0.5 d_I$. The effective grid spacing in the plane of the laser sheet was therefore $\Delta l/M = 3.28$ mm. A total of 2200 velocity vectors were typically obtained for each image.

III. Experimental Results

The development of the leading-edge vortex after cessation of the wing motion is represented by the instantaneous streamline patterns of Fig. 1 and the contours of constant vorticity of Fig. 2. The sectional streamline plot of Fig. 1a shows the abrupt onset of an antisymmetrical vortex arrangement characteristic of the helical mode of vortex breakdown. In Fig. 1b,

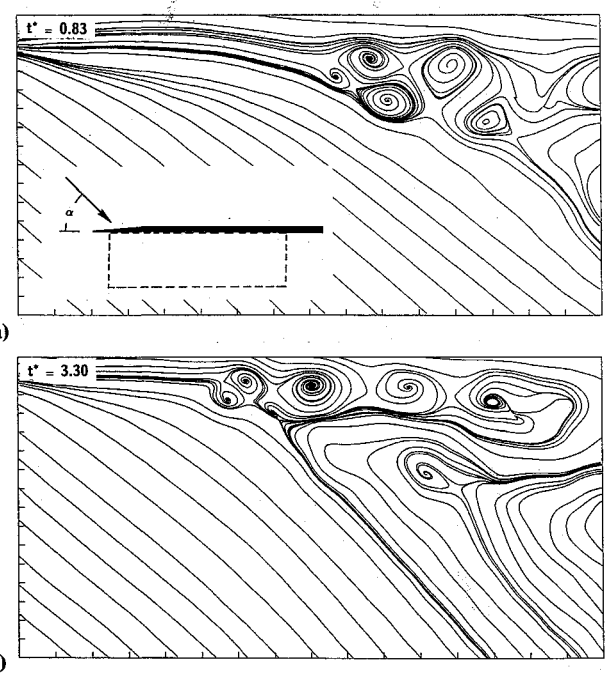

Fig. 1 Instantaneous sectional streamline pattern over a plane passing through the centerline of the leading-edge vortex at a) dimensionless time $t^* = tU/C = 0.83$ and b) $t^* = 3.30$ after cessation of pitching motion. Left and right sides of image correspond to distances from apex of wing of $x/C = 0.05$ and 0.93, respectively.

Received Aug. 8, 1992; revision received Oct. 2, 1992; accepted for publication Oct. 6, 1992.

*Research Assistant, Department of Mechanical Engineering and Mechanics.

†Paul B. Reinhold Professor, Department of Mechanical Engineering and Mechanics. Member AIAA.

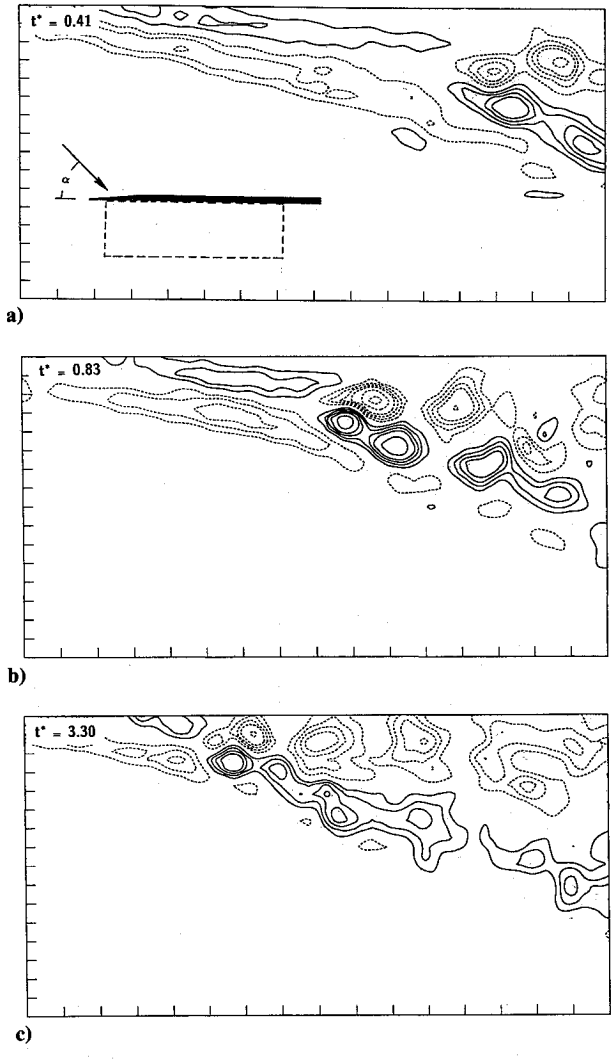

Fig. 2 Contours of constant positive (solid line) and negative (dashed line) vorticity over a plane passing through the centerline of the leading-edge vortex at a) dimensionless time $t^* = tU/C = 0.41$, b) $t^* = 0.83$, and c) $t^* = 3.30$. Left and right sides of image correspond to distances from apex of $x/C = 0.05$ and 0.93, respectively.

the apparent onset of instantaneous vortex breakdown has progressed upstream toward the apex, and the sectional streamline pattern is again of a form that suggests a helical mode of instability immediately after the onset of breakdown; however, this streamline pattern takes on a considerably more complex form over the right half of the image. Correspondingly, there is an abrupt increase in the width of the region of instantaneous reverse flow. Although these instantaneous, sectional streamline patterns provide a certain insight, instantaneous representations of the development of the vorticity field are essential.

The vorticity contours of Fig. 2a show that shortly after cessation of the motion, there is onset of the helical instability mode, represented by the staggered arrangement of the concentrations of negative (dashed line) and positive (solid line) vorticity. The onset of this instability occurs a significant distance upstream of the trailing edge, suggesting that the location of vortex breakdown moves upstream with a relatively high phase speed after cessation of the wing motion. Well-defined contours of relatively distributed positive and negative vorticity are apparent in the region upstream of the onset of the helical mode instability. A particularly important observation is that the sign of the azimuthal vorticity switches at the onset of vortex breakdown. That is, upstream of the onset of the instability, the positive, relatively distributed vorticity is located adjacent to the wing surface, whereas downstream of vortex breakdown, the negative, relatively concentrated vorticity is located closest to the wing surface. In fact, this basic criterion persists at the larger values of time shown in Figs. 2b and 2c. It is also of interest to note that the contours of constant vorticity upstream of the onset of vortex breakdown become more concentrated as the location of breakdown moves toward the apex of the wing.

This switch in sign of the azimuthal vorticity is in accord with the theoretical model of Brown and Lopez.[5] In essence, they show that the relation between the axial velocity $w(o, z)$ on the centerline of the vortex (at the axial location z) and the azimuthal vorticity η at radial location σ is

$$w(o, z) = \frac{1}{2}\int_{-\infty}^{\infty}\int_{0}^{\infty} \frac{\sigma^2\eta(\sigma, z')}{[\sigma^2 + (z - z')^2]^{3/2}}\, d\sigma\, dz'$$

Attainment of zero or negative velocity on the axis of the vortex is possible only if the azimuthal vorticity becomes negative. It should be noted that the switch in sign of the azimuthal vorticity at the onset of vortex breakdown, among other features, is clearly evident in the preliminary experiments described by Rockwell et al.[7] and the direct numerical simulation of Visbal.[6] It is evident from Figs. 2a–2c that the onset of negative azimuthal vorticity persists during the transient movement of the vortex breakdown region toward the apex of the wing. The total time interval between Figs. 2a and 2c corresponds to 2.93 convective time scales C/U, which is much larger than the time scale of the helical instability occurring at the onset of breakdown. It should be emphasized that the streamwise location of the switch in sign of azimuthal vorticity is not coincident with the location of the apparent stagnation point (i.e., onset of reverse flow), which is the traditional criterion typically based on steady or time-averaged representations of the breakdown process. Comparison of Figs. 1 and 2 shows that the onset of opposite-signed azimuthal vorticity occurs upstream of the apparent stagnation point, an observation also evident in the parallel numerical simulation of Visbal.[6]

Comparison of the sectional streamline patterns in Figs. 1a and 1b with the corresponding contours of constant vorticity of Figs. 2b and 2c show that, after the first few concentrations of azimuthal vorticity, the sectional streamlines do not provide an adequate representation of the concentrations of vorticity. That is, as evident in the right portion of the images of Figs. 2b and 2c, concentrations do exist, but their arrangement, as well as their values of circulation, are such that the sectional streamline patterns do not clearly indicate the presence of vortical structures.

Finally, inspection of the instantaneous streamline and vorticity contour plots at 20 closely spaced time intervals following the cessation of wing motion shows that the transverse extent of the large-scale separated zone downstream of vortex breakdown undergoes large undulations. Moreover, the apparent location of onset of vortex breakdown also exhibits a nonmonotonic variation with increasing time. These undulations, which tend to occur over a time scale of the order of one convective time scale C/U, are also accompanied by a switch in sign of the initially formed concentration of azimuthal vorticity. That is, a concentration of negative vorticity is first formed in Fig. 2a, whereas in Fig. 2b, it is the positive concentration that first appears. Further details of these undulations in relation to the onset of vortex breakdown and the large-scale separated zone downstream of it are addressed by Towfighi.[9]

IV. Conclusions

Particle image velocimetry allows effective characterization of the instantaneous structure of vortex breakdown in terms of contours of constant azimuthal vorticity and patterns of sectional streamlines. The nonstationary nature of the onset of vortex breakdown, as well as the decreasing coherence and increasing scale of the vortical structures with distance down-

stream of the onset of breakdown, are apparent by comparing images acquired at successive times. The concept of a switch in sign of the azimuthal vorticity at the onset of vortex breakdown is shown to be an essential feature of the vortex breakdown process. This criterion, first proposed in the theoretical model of Brown and Lopez,[5] persists during transient development of vortex breakdown following cessation of pitching motion of the wing.

Acknowledgments

This research program, sponsored by the Air Force Office of Scientific Research, was monitored by Major Daniel Fant.

References

[1]Hall, M. G., "Vortex Breakdown," *Annual Review of Fluid Mechanics,* Vol. 4, 1972, pp. 195–218.

[2]Leibovich, S., "The Structure of Vortex Breakdown," *Annual Review of Fluid Mechanics,* Vol. 10, 1978, pp. 221–246.

[3]Leibovich, S., "Vortex Stability and Breakdown: Survey and Extension," *AIAA Journal,* Vol. 22, No. 9, 1984, pp. 1192–1206.

[4]Escudier, M., "Vortex Breakdown: Observations and Explanations," *Progress in Aerospace Science,* Vol. 25, 1988, pp. 189–229.

[5]Brown, G. L., and Lopez, J. M., "Axisymmetric Vortex Breakdown. Part 2. Physical Mechanisms," *Journal of Fluid Mechanics,* Vol. 221, 1990, pp. 553–576.

[6]Visbal, M., "Structure of Vortex Breakdown on a Pitching Delta Wing," AIAA Paper 93-0434, Jan. 1993.

[7]Rockwell, D., Magness, C., Robinson, O., Towfighi, J., Akin, O., Gu, W., and Corcoran, T., "Instantaneous Structure of Unsteady Separated Flows via Particle Image Velocimetry," Dept. of Mechanical Engineering and Mechanics, Lehigh Univ., PI-1 Rept., Bethlehem, PA, Feb. 1992.

[8]Rockwell, D., Magness, C., Towfighi, J., Akin, O., and Corcoran, T., "High-Image-Density Particle Image Velocimetry Using Laser Scanning Techniques," *Experiments in Fluids,* Vol. 14, 1993, pp. 181–192.

[9]Towfighi, J., "Instantaneous Structure of Vortex Breakdown on a Delta Wing," M.S. Thesis, Dept. of Mechanical Engineering and Mechanics, Lehigh Univ., Bethlehem, PA, 1992.

Modified Solution for Finding the Optimal Angle of Spacecraft Walls Under Orbital Debris Impacts

Chris P. Pantelides* and Shyh-Rong Tzan†
University of Utah, Salt Lake City, Utah 84112

Introduction

In recent studies[1-3] it has been shown both analytically and experimentally that orbital debris impact is a hazard to long duration near-Earth space structures. In addition, it has been determined that most space debris impacts will occur at oblique angles to the surface of a space structure.[4] Experimental studies of oblique hypervelocity impact of multisheet structures have shown that there exists a critical debris particle trajectory angle beyond which projectile impacts produce ricochet debris that can cause major damage to orbiting structures.

Further experiments on modified dual-wall structural systems revealed that corrugated bumpers offer increased protection against perforation by hypervelocity projectiles compared to that obtained from monolithic bumpers.[3] A procedure was developed in Ref. 3 by which the configuration and the parameters of the corrugated bumper could be found to reduce the potential for creation of ricochet debris, in the event of an on-orbit impact. This Note presents a modification to the procedure in Ref. 3 in which one of the assumptions made in Ref. 3 is removed. It is shown that the optimal bumper rise angle depends on the ratio of ricochet debris velocity to spacecraft velocity (V_r/V_s ratio), has an asymptotic value of 45 deg, and is independent of the spacecraft orientation.

Received April 14, 1992; revision received Oct. 19, 1992; accepted for publication Oct. 29, 1992.

*Assistant Professor, Department of Civil Engineering.
†Research Assistant, Department of Civil Engineering.

Description of Oblique Hypervelocity Impact

A schematic of an oblique hypervelocity impact is shown in Fig. 1. Ricochet debris can be created in two ways: first, by the primary impact of the original projectile and, second, by the secondary impacts of ricochet debris on an adjacent corrugation face.[3] The parameters in Fig. 1 are defined as follows. Angle α is the rise angle of the corrugated bumper. Point 1 is the location of the primary impact of a projectile on the corrugated plate, and point 2 is the location of a secondary impact of a resulting ricochet particle. The angle between the normal to the bumper baseplate and the projectile trajectory is denoted by γ, and θ is the angle between the normal to the impacted face and the trajectory of the projectile. Note that γ is positive in the counter-clockwise direction and negative in the clockwise direction; θ is always positive. The velocity of the original projectile is V, and V_r is the velocity of the ricochet debris particle. The angle characterizing the trajectory of the ricochet debris particle with respect to the face that sustained the primary impact is denoted by η. The spacecraft orbital velocity is denoted as V_s, and ϵ is the angle between the velocity vector of the spacecraft and the normal to the bumper baseplate.

Optimal Angle of Corrugated Bumper Plate

The objective of the optimization is to find the angle α such that the amount of ricochet debris created by an oblique hypervelocity impact is minimized. Little or no ricochet debris is created when a projectile strikes a flat plate along a normal (or near normal) trajectory. To minimize the potential for ricochet debris creation, the normal components of the primary and secondary impacts must be maximized. The procedure used in the optimization is similar to that of Ref. 3.

Primary Impact

Using the terminology in Ref. 3 for the primary impact event, the normal velocity component is given as

$$V_{np} = V \cos\theta = 2\, V_s \cos\epsilon \cos\gamma \cos\theta \tag{1}$$

It is assumed that the particle impact velocity is twice the velocity component of the spacecraft normal to the bumper baseplate, based on the orbital environment. The sum of the normal components of all possible impacts on a pair of adjacent faces is

$$V_1 = \int_{-\pi/2}^{\pi/2} V_{np}\, \mathrm{d}\gamma \tag{2}$$

Figure 2 shows the four possible configurations for angle γ and the relationships between angles θ, α, and γ. Note that the four configurations in cases 5–8 of Fig. 2a are a mirror image of those for cases 1–4, so that only cases 1–4 need to be integrated (Fig. 2b). These can be written as

$$\theta = \gamma - \alpha \quad \text{if} \quad \alpha < \gamma < \pi/2 \tag{3a}$$

$$\theta = \alpha - \gamma \quad \text{if} \quad 0 < \gamma < \alpha \tag{3b}$$

$$\theta = \alpha - \gamma \quad \text{if} \quad \alpha - \pi/2 < \gamma < 0 \tag{3c}$$

$$\theta = -\gamma - \alpha \quad \text{if} \quad -\pi/2 < \gamma < \alpha - \pi/2 \tag{3d}$$

where $0 < \alpha < \pi/2$.